J Mater Sci (2009) 44:5919–5925
DOI 10.1007/s10853-009-3837-5

Synthesis and dielectric properties of $Ag(Nb_{0.6}Ta_{0.4})O_3$ ceramics prepared by solid-state and sol–gel methods

Lifeng Cao · Lingxia Li · Ping Zhang · Haitao Wu · Qingwei Liao

Received: 28 May 2009 / Accepted: 21 August 2009 / Published online: 2 September 2009

Abstract $Ag(Nb_{0.6}Ta_{0.4})O_3$ (ANT) ceramics were synthesized by conventional solid-state method and wet chemical method (sol–gel method). The effects of preparation methods on synthesis temperature, phase structure, morphology, Raman spectra, and dielectric properties of ANT ceramics were investigated. For sol–gel method, K_2CO_3 was used to dissolve Nb_2O_5 and Ta_2O_5, avoiding use of strong corrosive hydrofluoric acid. The results showed that the synthesis temperature of ANT phase obtained by sol–gel method was 700 °C, while that by solid-state method was 950 °C. The nanopowders around 40 nm were obtained by sol–gel method, while the micro-powders around 1.5 μm by solid-state method. In addition, the decrease of vibration frequency of $A_{1g}(O)$ stretch mode indicated that the Nb–O or Ta–O bonds became weak, which lead to high permittivity. The dielectric properties of the ceramics prepared by the two methods were different. Notably, the dielectric loss (6.6×10^{-4}) of ANT ceramic synthesized by sol–gel method was much lower than that (22.8×10^{-4}) by solid-state method.

Introduction

The perovskite-type ceramics have received considerable attention due to their excellent properties in catalytic, electronic, and ion exchange applications [1]. The perovskite-type $Ag(Nb,Ta)O_3$ ceramic possesses excellent properties, low dielectric losses ($<18 \times 10^{-4}$) combined with an extraordinary high permittivity (>430), which makes it potentially useful for wireless-communication, microelectronic technologies, and miniaturization of microwave components [2–4]. Many researches have been carried out to investigate how to improve its dielectric properties by conventional solid-state reaction method [5–8]. However, this conventional method involves high calcination temperature and repeated cycles of milling, which resulting in the loss of the fine powder nature. In addition, the powder prepared by solid-state reaction method usually displays larger grain sizes and lower sinterability [9, 10]. In comparison with conventional solid-state method, sol–gel method is an excellent technique for offering a better chemical homogeneity and low-temperature processing. It also allows the control of the chemical pore size distribution of the nanoparticulate materials [11–13]. Sol–gel method is considered to be a promising way to produce high-purity and phase-pure powders [14].

However, $Ag(Nb,Ta)O_3$ powders synthesized by sol–gel method were seldom reported [15]. And there is no report about the dielectric properties of $Ag(Nb,Ta)O_3$ ceramics prepared by sol–gel method. At present, as raw materials for synthesizing $Ag(Nb,Ta)O_3$ powders, Nb_2O_5 and Ta_2O_5 are decomposed by concentrated hydrofluoric acid (HF). The main disadvantage of this approach is that it requires special container due to the great corrosiveness of HF. Moreover, the decomposition process results in the loss of a considerable amount of HF because of volatilization, which brings great harm to human beings and equipments.

From the analysis of the dielectric properties of $AgNbO_3$–$AgTaO_3$ system performed by Kania [16], we can see that around room temperature and in the

L. Cao · L. Li (✉) · P. Zhang · H. Wu · Q. Liao
School of Electronic and Information Engineering, Tianjin University, Tianjin 300072, China
e-mail: lilingxia@tju.edu.cn

L. Cao
e-mail: clf198044@126.com

H. Wu
School of Materials Science and Engineering, University of Jinan, Jinan 250022, China

composition of $Ag(Nb_{0.6}Ta_{0.4})O_3$ the temperature coefficient of capacitance (TCC) somewhat flattens. In addition, the permittivity of $Ag(Nb_{0.6}Ta_{0.4})O_3$ composition is the highest in $Ag(Nb_{1-x}Ta_x)O_3$ ($x = 0$–1) systems around room temperature. These are the reasons why we focused on this particular composition. In this study, $Ag(Nb_{0.6}Ta_{0.4})O_3$ ceramics were synthesized by sol–gel method with the assistance of K_2CO_3, avoiding use of HF based on our previous work [17]. The effects of the solid-state and sol–gel methods on synthesis temperature, phase structure, morphology, Raman spectra, and dielectric properties of ANT ceramics were investigated.

Experimental

Conventional solid-state preparation for ANT ceramics

High-purity powders of Nb_2O_5 (99.99%, Nonferrous Metal Refiring Factroy, China), Ta_2O_5 (99.99%, Nonferrous Metal Refiring Factroy, China), and Ag_2O (99.99%, Beijing Chemical Corp., China) were used to prepare $Ag(Nb_{0.6}Ta_{0.4})O_3$ (ANT) ceramic. They were weighed according to the stoichiometric ratio and mixed by ball-milling in distilled water for 8 h. The dried mixtures were then put into corundum crucibles and heated at 1050 °C for 10 h in air.

Sol–gel preparation for ANT ceramic

Nb_2O_5, Ta_2O_5, $AgNO_3$ (99.0%, Kewei limited company, China), and K_2CO_3 (90.0%, Kewei limited company, China) were used as raw materials. The synthesis procedure was shown as follows: Nb_2O_5, Ta_2O_5, and K_2CO_3, with mol ratio of 1:1:18 reacted at 900 °C to form mixture of K_3NbO_4 and K_3TaO_4. After the mixture was dissolved in distilled water, the solutions were set at pH < 5 to form precipitates, $Nb(OH)_5$ and $Ta(OH)_5$, completely. Then niobium citrate and tantalum citrate formed after the filtered-off precipitates were dissolved in citrate acid (CA). Silver citrate was also obtained when stoichiometric $AgNO_3$ was dissolved in citrate acid. The molecularly modified precursor's hydrolysis reacted subsequently, and the organic mixture containing niobium, tantalum, silver precursors, and ethylene glycol (EG) was mixed and stirred to produce an Ag–Nb–Ta complex solution. The mol ratio of CA and EG was 1:4. By heating in a water bath at 100 °C, a gel was formed after evaporation of water. Subsequently, powders were obtained after the gel was calcined at 750 °C for 1 h in air.

The powders synthesized by solid-state method were mixed using de-ionized water and zirconia milling media for 8 h. The powders prepared by the two different methods were granulated by mixing them in a 7 wt% poly (vinyl) alcohol (PVA) solution, and then the granules were pressed into disks with 10 mm in diameter and 1–1.5 mm in thickness under a pressure of 10 MPa. These samples were sintered at a temperature range of 1050–1180 °C for 4 h in air, with the heating rate of 5 °C/min and followed natural cooling.

Characterization methods

Thermal behavior of powder and gel was examined by means of thermogravimetric (TG) (STA409EP, Netzsch, Germany). Phase analysis was conducted by X-ray diffractometer (D/MAX-B, Rigaku co., Japan) with Cu $K\alpha$ radiation at 40 kV and 40 mA settings. Morphology of materials was observed by a field emission scanning electron microscope (FE-SEM) (Nanosem 430, FEI Co., USA). The capacitance and dielectric loss were measured at 1 MHz with a capacitance meter (HP4278A). The dependence of permittivity on temperature was measured with a GZ-ESPEC oven and HM 27002 C-T Meter Model. The sintered densities of ANT samples were measured by Archimedes method (XS64, Mettler Toledo, Switzerland). Raman measurements were carried out at room temperature, and the signals were recorded by a Bruker FS100 triple-gaining Raman spectrometer, equipped with a liquid-nitrogen-cooled CCD. The 100-mW output of the 1064-nm line of a Nd YAG laser was used as the excitation source. The obtained Raman spectra were recorded with a resolution approximately 2 cm^{-1}.

Results and discussion

Study of phase formation

Figure 1a presents TG curves of the powder prepared by solid-state method. From 0 to 441 °C, the mass loss of about 4.43% was observed, which was due to the H_2O loss and the release of oxygen from Ag_2O [18]. From 441 to 931 °C, a weight gain was observed, which indicated that the ANT phase formation began at about 441 °C and then finished around 931 °C. Figure 1b shows the TG curves of the dried gel (200 °C) prepared by sol–gel method. It was shown that there were two stages of weight loss. The first stage (below 230 °C) with a slow weight loss was related to elimination of structure water and the vaporization of residual organic acid and ethylene glycol. The second stage (230–565 °C) with weight loss of about 67.13% was related to the decomposition and oxidation of organic compounds. At 680 °C, there was no weight loss, indicating the crystallization of ANT. Therefore, it indicated that ANT phase could be synthesized around 700 °C.

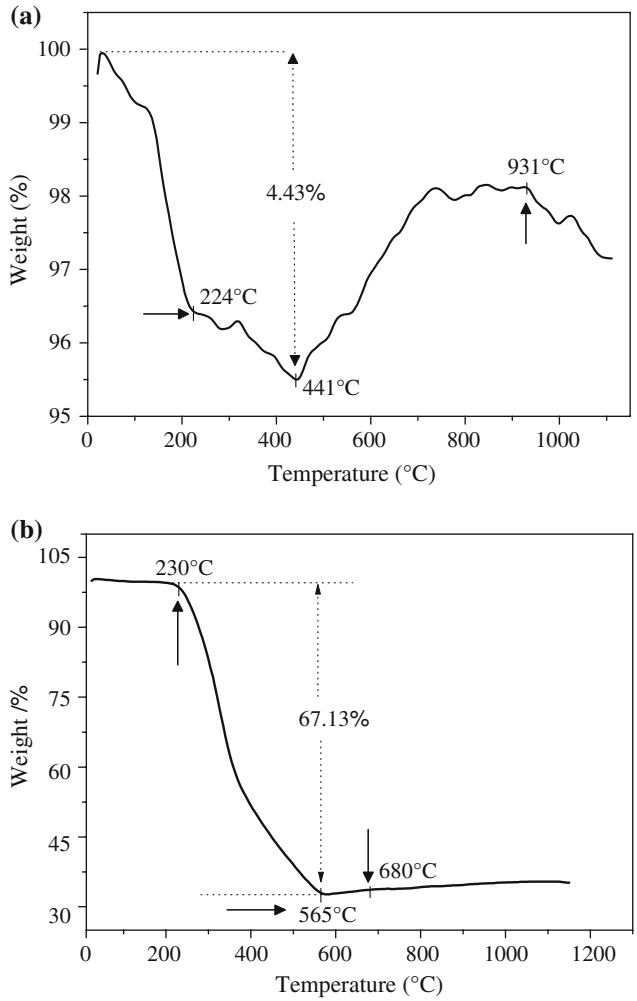

Fig. 1 TG curves of ANT powders synthesized by **a** solid-state method, and **b** sol–gel method

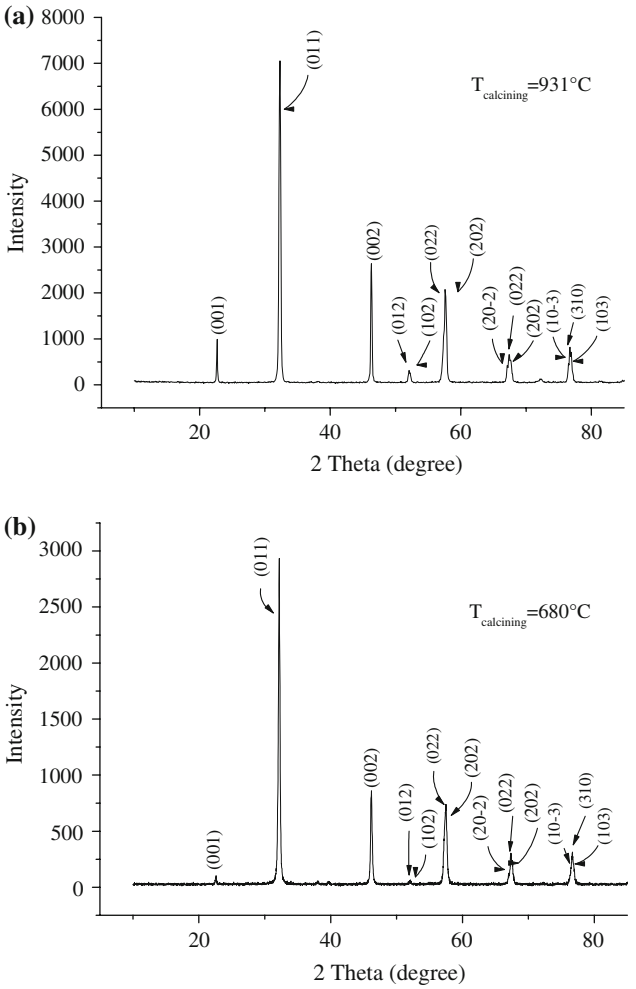

Fig. 2 XRD patterns of ANT powders prepared by **a** solid-state method (at 950 °C), and **b** sol–gel method (at 700 °C)

XRD analysis performed on calcined sample is shown in Fig. 2. The ANT powders prepared by solid-state and sol–gel method were heat treated at 950 and 700 °C, respectively. The pure perovskite phase was found for samples prepared by solid-state and sol–gel methods and their unit cell matched that of monoclinic ANT in *P2/m* space group as presented in JCPDS file no. 51-0373. These results suggested that the synthesis temperature of ANT phase obtained by sol–gel method was much lower than that by solid-state method.

Lattice distortion

According to the theory of X-ray diffraction, the relation between the interplanar spacings d_{hkl} and the diffraction angle can be expressed as follows:

$$\lambda = 2d_{hkl}\sin\theta \tag{1}$$

For monoclinic structure, the lattice parameter of a given plane with Miller indices (*hkl*) can be derived using the equation [19]:

$$\frac{1}{d_{hkl}^2} = \frac{h^2}{a^2\sin^2\gamma} + \frac{k^2}{b^2\sin^2\gamma} + \frac{l^2}{c^2} - 2hk\frac{\cos\gamma}{ab\sin^2\gamma} \tag{2}$$

where a, b, c, and γ are lattice parameters. The results of the calculations for the various samples were presented in Table 1. Sample A was prepared by solid-state method

Table 1 XRD results for the ANT samples synthesized by *A* solid-state method, and *B* sol–gel method

Samples	2θ	d_{hkl} (Å)	a	b	c	V (Å^3)
A	32.348	2.7653	3.92860	3.92590	3.93020	60.61
B	32.179	2.7794	3.93326	3.92929	3.93146	60.76

while sample B by sol–gel method. All these calculations were performed automatically by programme.

For the sample prepared by sol–gel method, the XRD results showed that the peak positions of (011) diffraction lines, as well as other ones, shifted to lower angles with decreasing grain size. With the decrease of average grain sizes, both the lattice parameter and the unit cell volume V increased. The lattice distortion of ANT nanopowders prepared by the sol–gel method was combined with the interfacial energy and surface tension mutual attraction of the nanopowders [20, 21].

Morphology

Figure 3 gives the FE-SEM photographs of ANT powders and ceramics synthesized by the solid-state method and sol–gel method, respectively. It was observed that the powder sizes prepared by solid-state method were around 1.5 μm (Fig. 3(a1)) while those by sol–gel method around 40 nm (Fig. 3(b1)). This morphology affirmed our suggestion of the micro-powders and nanopowders prepared by solid-state method and sol–gel method, respectively. The powder size obtained by sol–gel method in this work was similar to that reported by Song et al. [22].

Figure 3(a2) shows microstructure of ANT ceramic synthesized by solid-state method. The sample exhibited the microstructure with grain sizes around 5 μm and a density of 7.381 g/cm^3 at sintering temperature (1160 °C). And the increase of sintering temperature (e.g., 1180 °C) could not improve densification, because of evaporation of silver (Fig. 4). Figure 3(b2) presents morphology of ANT ceramic synthesized by sol–gel method. The sample exhibited the microstructure with grain sizes around 1 μm and a density of 7.674 g/cm^3 at 1050 °C. It indicated that the decrease of powder sizes was helpful to densification of the ceramics. Comparing with the density of the ceramics prepared by the two methods, it concluded that the obtaining of high density of the ceramic prepared by sol–gel method at low sintering temperature was due to the surface activity of nanopowders.

Dielectric properties

Figure 5 shows the permittivity and dielectric loss of ANT ceramics prepared by solid-state method and sol–gel method, respectively. The error bars indicated the standard deviation resulted from the dielectric loss and permittivity measurement. The permittivity increased while the dielectric loss decreased for both samples with sintering temperature increasing. However, the most excellent dielectric properties of the sample prepared by solid-state method were obtained at 1160 °C while those obtained by sol–gel method at 1050 °C. These results suggested that the sintering temperature of ANT samples prepared by sol–gel method was lower than that by solid-state method (from 1160 down to 1050 °C). Notably, the dielectric loss

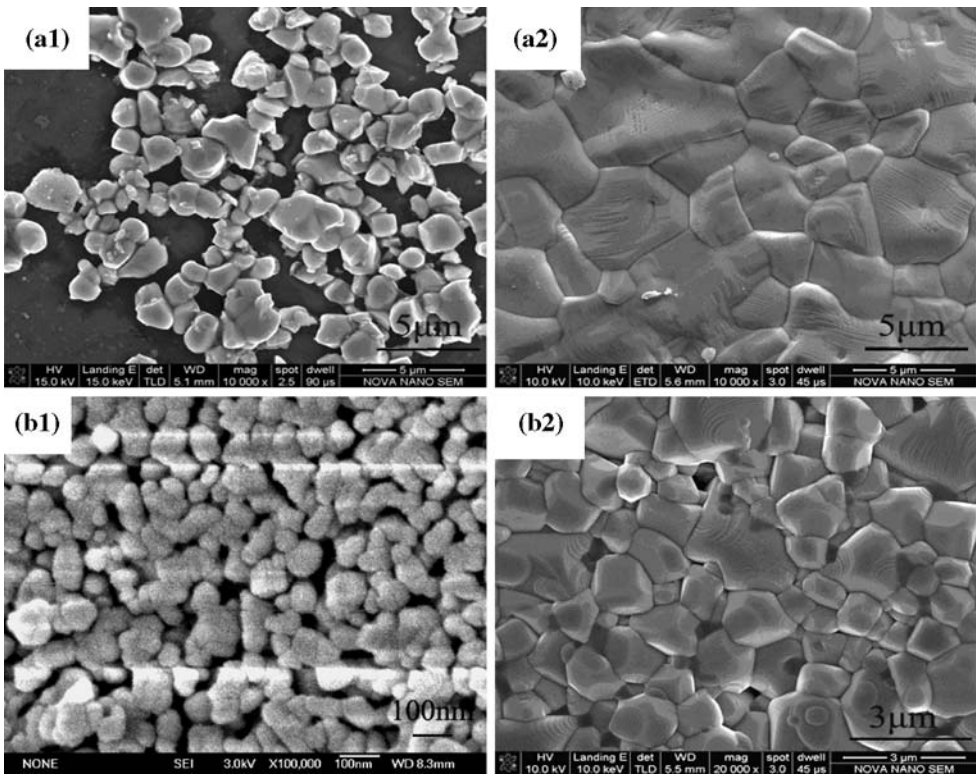

Fig. 3 Micrographs of ANT powders and ceramics: **a1** and **a2** were prepared by solid-state method, and **b1** and **b2** were prepared by sol–gel method

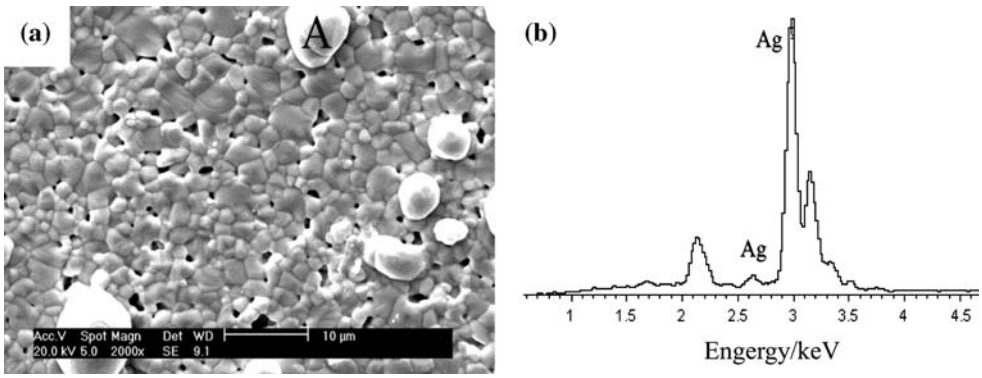

Fig. 4 SEM and EDS of sintered (at 1180 °C) ANT ceramic prepared by solid-state reaction method: **a** SEM of the sample, and **b** EDS of point A in **a**

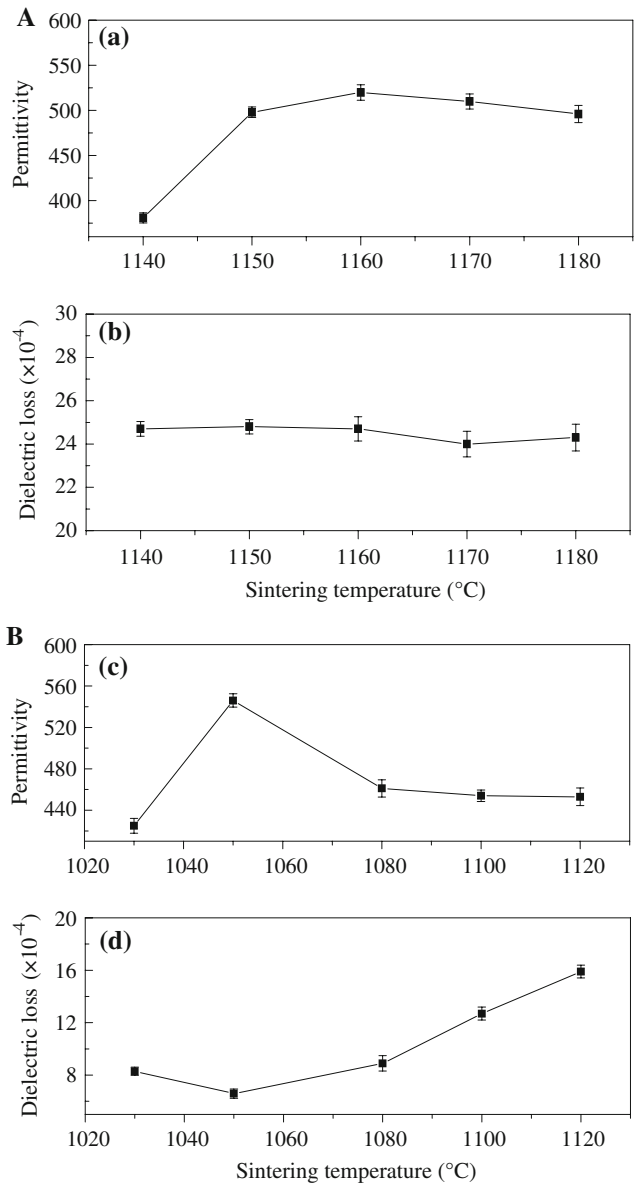

Fig. 5 Dielectric properties of ANT ceramics synthesized by **A** solid-state method, and **B** sol–gel method

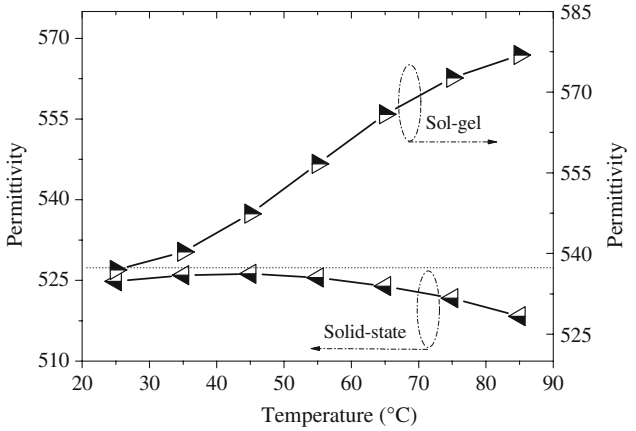

Fig. 6 Permittivity dependence on temperature for samples prepared by solid-state method and sol–gel method

(6.6×10^{-4}) of ANT ceramic synthesized by sol–gel method was much lower than that (22.8×10^{-4}) by solid-state method. These results indicated that the ceramics synthesized by sol–gel route promised low synthesis temperature and good dielectric properties as the mixing took place at atomic level and free from contamination, since no grinding media were involved.

Figure 6 shows the dependence of permittivity on temperature for samples prepared by the two methods. There was an imperceptible change in permittivity dependence on temperature for the sample synthesized by solid-state method, which was consistent with that reported by Kania [16]. However, the permittivity of the sample for sol–gel method increased obviously with the increase of temperature. These different variation tendencies might be due to the variations of elastic coefficient that caused by the change of lattice constant [23].

Raman spectra

Generally, the Raman spectroscopy can provide important information that correlates the vibration characteristics of

the materials with the microwave dielectric properties, even though the Raman phonons of the complex perovskite materials are mainly non-polar [24]. Though many researches on the Raman scattering of niobates, tantalates or $Ag(Nb,Ta)O_3$ have been reported [25–27], the correlation on Raman scattering and dielectric properties was scarcely reported [7].

In our experiment, Raman scattering spectra of ANT ceramics synthesized by the two preparation methods are shown in Fig. 7. The vibrations are classified as internal modes of the $(Nb,Ta)O_6$ octahedra and lattice translations involving motion of the cation [25]. The bands at $<200\ cm^{-1}$ were associated with the Ag^+ translational mode and the rotation of the $(Nb,Ta)O_6$ octahedra [28, 29]. The assignment of the active frequencies in Raman spectroscopy was proposed by many authors [30, 31]. The $(Nb,Ta)O_6$ octahedron with O_h symmetry has six fundamental vibrations: $\nu_1(A_{1g}) \rightarrow A_1$; $\nu_2(E_g) \rightarrow A_1 + A_2$; ν_3, ν_4 $(F_{1u}) \rightarrow A_1 + B_1 + B_2$; $\nu_5(F_{2g}) \rightarrow A_1 + B_1 + B_2$; $\nu_6(F_{1u}) \rightarrow A_2 + B_1 + B_2$. All modes are Raman active and all except the A_2 modes are infrared active. Raman peaks, near 205 and 246 cm^{-1}, were assigned to E_g(Nb/Ta) and A_{1g}(Nb/Ta) modes, which were due to the first-order scattering induced by niobium [32]. Two modes associated with the vibration of O atoms at 417.8 cm^{-1} was F_{2g}(O) and near 552 cm^{-1} was E_g(O) modes. The broad peak near 810 cm^{-1}, which corresponds to A_{1g}(O) was the stretch mode of the oxygen octahedron.

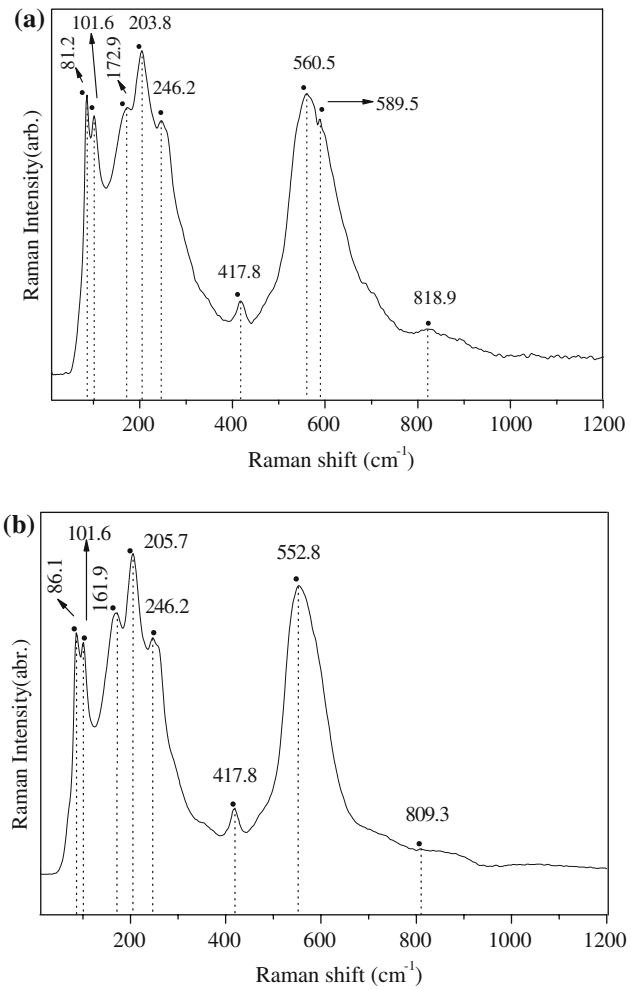

Fig. 7 Raman spectrum of ANT ceramics synthesized by **a** solid-state method, and **b** sol–gel method

The vibration frequency of Raman peaks at 560.5 and 589.5 cm^{-1} of ANT ceramic prepared by solid-state method was higher than that ($\sim$552 cm^{-1}) by sol–gel method. Compared with the Raman character obtained by solid-state method, the two peaks of the ceramic around 570 cm^{-1} synthesized by sol–gel method overlapped. The oxygen-octahedron stretch mode around 810 cm^{-1} [A_{1g}(O)] of ANT ceramic prepared by sol–gel method shifted to lower vibration frequency than that by solid-state method. Additionally, the peak became broad and weak (Fig. 7b) which indicated that the distortion of oxygen octahedron was induced. These suggested that the strength of Nb–O or Ta–O bonds became weak. According to the results of XRD, the average bond length in $(Nb,Ta)O_6$ octahedra of ANT ceramics synthesized by solid-state and sol–gel method was 1.9608 and 1.9624 Å, respectively, which was consistent with that discussed above. This concluded that the obtaining of the high permittivity of the sample prepared by solid-state method was due the looseness of the $(Nb,Ta)O_6$ octahedra cages.

Conclusions

Pure ANT phases were obtained by both conventional solid-state reaction method and sol–gel method. The character and dielectric properties of the ANT ceramics synthesized by the two different methods were investigated. The results showed that the synthesis temperature of ANT phase prepared by sol–gel method was much lower than that by solid-state method. In addition, micro-powders with size around 1.5 μm were obtained by solid-state method, while nanopowders around 40 nm by sol–gel method. The XRD results suggested that the lattice parameter and unit cell increased with the decrease of average grain size, which was due to the interfacial energy and mutual surface tension attraction of the nanopowders. There was an imperceptible change in permittivity dependence on temperature for sample prepared by solid-state method while obvious change for that by sol–gel method. As to the Raman spectra of ANT ceramic synthesized by sol–gel method, the vibration frequency of A_{1g}(O) stretch mode shifted to low wavenumber, which indicated that the distortion of oxygen octahedra was strengthened. This

phenomena also suggested the correlation between the permittivity and the rigidity of the (Nb,Ta)O_6 octahedra. Additionally, the low dielectric loss of ANT ceramics illustrated the advantages of sol–gel method.

Acknowledgements This work was supported by Program for New Century Excellent Talents in University (NCET) and 863 program (2007AA03Z423) and China Postdoctoral Science Foundation.

References

1. Ratheesh R, Sreemoolanadhan H, Sebastian MT (1997) J Solid State Chem 131:2
2. Valan M, Suvorov D, Hoffmann C, Sommariva H (2001) J Eur Ceram Soc 21(15):2647
3. Valant M, Suvorov D (1999) J Am Ceram Soc 82(1):88
4. Kim H, Shrout T, Randall C, Lanagan M (2002) J Am Ceram Soc 85(1):2738
5. Hu X, Valant M, Suvorov D (2006) J Appl Phys 99:124109
6. Li LX, Zhao J, Zhang P (2007) J Rare Earth 25:163
7. Guo XY, Zhu N, Xiao M, Wu XW (2007) J Am Ceram Soc 90(8):2467
8. Li LX, Wu XW, Wang YM (2003) J Electroceram 11(3):163
9. Khamman O, Tan X, Ananta S, Yimnirun R (2009) J Mater Sci 44:1868. doi:10.1007/s10853-008-3235-4
10. Duguey S, Lebourgeois R, Ganne JP, Heintz JM (2007) J Eur Ceram Soc 27:1087
11. Cheng JZ, Yang H, Yu LX, Xu W (2008) J Mater Sci: Mater Electron 19:442
12. Garbout A, Bouattour S, Botelho do Rego AM, Ferraria A, Kolsi AW (2007) J Cryst Growth 304:374
13. Xu YB, He YY, Chen XM, Zhang XB, Wang LB (2002) J Mater Sci: Mater Electron 13:197
14. Wang SF, Gu F, Lü MK, Song CF, Liu SW, Xu D, Yuan DR (2003) Mater Res Bull 38:1283
15. Song KX, Yan YQ, Li JH, Wang JP (2004) J Tianjin Univ 37:1019
16. Kania A (1983) Phase Transit 3:247–258
17. Cao LF, Li LX, Zhang P, Wu HT (2009) J Sol–Gel Sci Technol 51:251
18. Gernea M, Monnereau O, Llewellyn P, Tortet L, Galassi C (2006) J Eur Ceram Soc 26:3241
19. Yu YN (2006) Fundamentals of material science. Higher Education, Beijing
20. Wei ZQ, Xia TD, Ma J, Feng WJ, Dai JF, Wang Q, Yan PX (2007) Mater Charact 58:1019
21. Ye XS, Sha J, Jiao ZK, Zhang L (1999) Funct Mater 29(3):287
22. Song KX, Li JH, Xiao M, Yan YQ, Wang JP (2005) Chin J Inorg Chem 21:273
23. Zheng JQ (1978) J South China Univ Technol 6:22
24. Chih CT, Chen YC, Cheng HF (2003) J Appl Phys 94:3360
25. Kugel GE, Fontana MD, Hafid M, Roleder K, Kania A, Pawelczyk M (1987) J Phys C Solid State Phys 20:1217
26. Kania A, Roleder K, Kugel GE, Fontana MD (1986) J Phys C Solid State Phys 19:9
27. Hafid M, Kugel GE, Kania A, Roleder K, Fontana MD (1992) J Phys Condens Matter 4:2333
28. Ross SD (1970) J Phys C Solid State Phys 3:1785
29. Shen ZX, Kuok XB, Tang MH (1998) J Raman Spectrosc 29:379
30. Kakimoto K, Akao K, Guo Y, Ohsato H (2005) Jpn J Appl Phys 44:7064
31. Rousseau DL, Bauman RP, Porto SPS (1981) J Raman Spectrosc 10:253
32. Hu YM, Gu HS, Hu ZL, Wang H (2007) J Colloid Interface Sci 310:292